WESTERN OCEANUS PROCELLARUM AS SEEN BY C1XS ON CHANDRAYAAN-1

S.Z. Weider[1,2,3*], K.H. Joy[4], I.A. Crawford[1,2], B.J. Kellett[6], B.M. Swinyard[6,7] & C.J. Howe[6]

[1] Department of Earth and Planetary Sciences, Birkbeck College, Malet Street, London WC1E 7HX, UK.

[2] Centre for Planetary Science at UCL/Birkbeck, University College London, Gower Street, London WC1E 6BT, UK.

[3] Department of Terrestrial Magnetism, Carnegie Institution of Washington, Washington DC 20015, USA.

[4] School of Earth, Atmospheric and Environmental Sciences, University of Manchester, Williamson Building, Oxford Road, Manchester, M13 9PL, UK.

[6] RAL Space, Rutherford Appleton Laboratory, Didcot, Oxon OX11 0QX, UK.

[7] Department of Physics and Astronomy, UCL, Gower Street, London WC1E 6BT, UK.

* Corresponding author. Email: sweider@ciw.edu.

Keywords

Moon, surface; Regoliths; Gamma-ray spectroscopy

Abstract

We present the analysis of an X-ray fluorescence (XRF) observation of the western part of Oceanus Procellarum on the Moon's nearside made by the Chandrayaan-1 X-ray Spectrometer on 10th February 2009. Through forward modelling of the X-ray spectra, we provide estimates of the MgO/SiO_2 and Al_2O_3/SiO_2 ratios for seven regions along the flare's ground track. These results are combined with FeO and TiO_2 contents derived from Clementine multispectral reflectance data in order to investigate the compositional diversity of this region of the Moon. The ground track observed consists mainly of low-

Ti basaltic units, and the XRF data are largely consistent with this expectation. However, we obtain higher Al_2O_3/SiO_2 ratios for these units than for most basalts in the Apollo sample collection. The widest compositional variation between the different lava flows is in wt % FeO content. A footprint that occurs in a predominantly highland region, immediately to the north of Oceanus Procellarum, has a composition that is consistent with mixing between low-Ti mare basaltic and more feldspathic regoliths. In contrast to some previous studies, we find no evidence for systematic differences in surface composition, as determined through X-ray and gamma-ray spectroscopy techniques.

1. Introduction

1.1. Oceanus Procellarum

Oceanus Procellarum, in the western hemisphere of the Moon, is the largest of the lunar maria. Its numerous lava flow deposits are highly diverse in composition and eruption age (*e.g.,* Pieters, 1978; Wilhelms et al., 1987; Hiesinger et al., 2003; Hackwill et al., 2006). The Oceanus Procellarum deposits have inferred crater-count ages that span from the early stages of mare volcanism (~3.6 Ga) through to the potentially youngest (~1.2 Ga) basalts on the lunar surface (Hiesinger et al., 2003). The region, therefore, provides an opportunity to investigate the temporal evolution of lunar volcanism and the Moon's thermal history. The wide range of TiO_2 abundance in the Apollo and Luna mare basalt samples serves as the primary basis for their chemical classification (Neal and Taylor, 1992). These samples provide ground truth information for the remote sensing campaigns that allow geochemical and compositional mapping of unsampled regions of the Moon. There does not appear to be a simple correlation between the age and composition of lava flows on the lunar surface (*e.g.,* Pieters, 1978; Giguere et al., 2000; Hiesinger et al., 2003, 2011). However, spectral reflectance data for late stage lava flows on the western nearside indicate that they have high TiO_2 contents (Charette et al., 1974; Pieters, 1978; Johnson et al., 1991; Blewett et al., 1997; Davis, 1980; Elphic et al., 2000, 2002) and a significant olivine component (Pieters et al., 1980; Staid et al., 2011).

1.2. C1XS

The Chandrayaan-1 X-ray Spectrometer (C1XS) was a compact X-ray spectrometer (Grande et al., 2009a; 2009b; Howe et al., 2009) onboard the Chandrayaan-1 mission (Bhandari, 2005; Goswami and Annadurai, 2009) and was designed to measure the abundance of major rock-forming elements (*e.g.,* Mg, Al, Si, Ca, Ti, and Fe) in the lunar surface. One of the major scientific objectives (Crawford et al., 2009) was to provide new independent measurements of the composition of the mare basalts and thereby help constrain the thermal and chemical evolution of the lunar mantle. The premature end to the Chandrayaan-1 mission, coupled with low solar activity during its lifetime, meant that this objective was only partially fulfilled. However, data for basaltic regions were obtained from swaths through Mare Serenitatis, and through Mare Insularum, Mare Cognitum, and Mare Nubium (Weider et al., 2012a), as well as for a ground track through the western part of Oceanus Procellarum, which we analyse in this paper. In addition, an observation over a portion of the south-central nearside highlands was analysed by Narendranath et al. (2011).

1.3. Planetary XRF

Planetary X-ray fluorescence (XRF) is the process in which X-rays emitted from the Sun during flare events interact with atmosphere-less bodies in the inner Solar System and cause ionisation of atoms within the top ~100 μm of the regolith (*e.g.,* Yin et al., 1993; Clark and Trombka, 1997). The resulting fluorescent X-rays, with characteristic energies, can be measured by an orbiting XRF spectrometer (*e.g.,* C1XS). Analysis of the resulting X-ray spectra can be used to map the abundance of major elements such as Mg, Al, and Si (also Ca, Ti, and Fe during strong solar activity) on the planetary surface. Planetary XRF missions include an additional detector to simultaneously measure the incident solar X-ray flux, which varies on short timescales. C1XS was accompanied on Chandrayaan-1 by the X-ray Solar Monitor (XSM) for this purpose. Full descriptions of both these instruments and their calibrations have been published previously in a suite of

papers (Huovelin et al., 2002; Alha et al., 2009; Howe et al., 2009; Narendranath et al., 2010).

1.4. Geologic context of observation

Lunar XRF from a B-class (10^{-7} to 10^{-6} Wm^{-2}) solar flare on 10th February 2009 was observed by C1XS. This observation had an ~1800 km-long ground track (full width footprint of ~50 km) through western Oceanus Procellarum at a longitude of ~290° (Figure 1). No previous lunar XRF instrument (e.g., on Apollo 15 and 16) has mapped this region of the Moon's surface. At its finest resolution (based on counting statistics), the observation can be divided into seven spatially resolved regions that run through western Oceanus Procellarum and into an area of highlands to the north of the maria. This provides an opportunity to study the major element composition and evolution of mare basalts over a number of separate lava flows. The ground track falls mainly within the outer band of concentric (according to Wilhelms et al., 1987) Procellarum mare deposits. These consist of Upper Imbrian (~3.5 Ga), mostly low-Ti (~3 wt% TiO_2) basalts. Clementine multispectral reflectance data show that the ground track is more variable in FeO (Figure 1b) than TiO_2 (Figure 1c) content. The FeO concentration varies from ~6 wt% in the northern (highlands) region to ~18 wt% in the basaltic area. FeO and TiO_2 values are derived using the algorithms of Gillis et al. (2004) and Gillis et al. (2003), respectively. We obtained and processed the data from the Lunar and Planetary Institute's Clementine Mapping project (http://www.lpi.usra.edu/lunar/tools/clementine/) and our own in-house IDL (Interactive Data Language) code. The FeO variation within the flare's ground track is therefore more representative of the lithological diversity in Oceanus Procellarum.

2. Data and spectral modelling

Raw X-ray flux data during the C1XS observation on 10th February 2009 (between 23:07:54 and 23:25:09 U.T.) were collected in the time-tagged single pixel mode (see Howe et al., 2009), converted to 16 s binned spectra, and then calibrated using pre-flight

and in-flight calibration information (Narendranath et al., 2010), and instrument housekeeping data. Flux from each of the 24 instrument detectors were co-added in order to obtain sufficient signal to noise ratios. The ground track has been split into seven regions of interest (ROI), as shown in Figure 1. The boresight locations of each ROI are given in Table 1 and the spectra are shown in Figure 2. Detector background levels, determined during quiet sun periods, were subtracted from the seven individual spectra and the resultant spectra (Figure 2) were forward modelled using the *RAL abundance algorithm* (Weider et al., 2011). This algorithm employs a modified fundamental parameters approach (*e.g.,* He and Van Espen, 1991) based on the methods of Clark and Trombka (1997); it has been described by Swinyard et al. (2009) and Weider et al. (2011) and shown to successfully replicate ground truth information for a C1XS observation of the Apollo 14 landing site (Weider et al., 2012a). The algorithm requires several inputs: (i) the modelled solar spectrum, (ii) the efficiency of the C1XS instrument, (iii) an arbitrary initial rock composition, and (iv) the phase angle of the observation. These parameters and the methodology we employed for this analysis are fully described by Weider et al. (2012a).

2.1 Si normalisation

In the RAL abundance algorithm the modelled spectrum is normalised to the XRF data using the total counts within the Si K_α peak. This normalisation is possible because the Si concentration of most lunar soils and regolith breccias is within a narrow range of 18–23 elemental wt % (*e.g.,* Rhodes and Blanchard, 1981; Fruland, 1983; Morris et al., 1983; Simon et al., 1985; McKay et al., 1986, 1989; Jerde et al., 1987, 1990). All other elemental abundances are therefore assessed against the fixed Si (21 wt %; Prettyman et al., 2006) and are expressed as elemental ratios (*i.e.,* Mg/Si and Al/Si). This normalisation largely cancels out inaccuracies in the results caused by calibration uncertainties and variations in XRF intensity that are related to physical and compositional heterogeneities in the regolith (Clark and Trombka, 1997; Maruyama et al., 2008; Näränen et al., 2008; Weider et al., 2011). Theoretical and experimental investigations of XRF geometry effects (e.g., Maruyama et al., 2008; Näränen et al.,

2008; Parvianen et al., 2011; Weider et al., 2011) have shown that it can be problematic to express XRF-derived abundances as ratios of two elements that differ significantly in energy (e.g., Si and Fe). However, we present results only for ratios of elements that have similar X-ray energies and so our results are not subject to any phase angle effects. It is important to note that normalisation with respect to Si has only a minor effect on the uncertainties for the Mg and Al results, which are instead completely dominated by the lack of a direct measure of the incident solar flare spectrum (see below).

2.2 Flare temperature estimate

Although XSM was flown onboard Chandrayaan-1 (see Section 1.3.) to provide a direct measure of the incident solar spectrum, the flare described here was below its minimum detection capabilities and therefore an alternative source of a suitable solar spectrum was required. We used data from GOES-10 (Geostationary Operational Environment Satellite) to estimate a range of likely flare plasma temperatures, as in Weider et al. (2012a). We then used the *atomdb* (version 2.0.0) database and modelling software (Harvard Chandra X-ray Center: http://cxc.harvard.edu/atomdb/features_idl_html) to generate high-resolution modelled solar spectra with bremsstrahlung continuum and superimposed emission lines for equivalent temperatures (the software only tabulates data at certain, discrete, temperatures). The GOES long-wavelength (1–8 Å) channel intensity during the flare peaks at 1.37×10^{-7} Wm^{-2} (see Figure 3). This occurred simultaneously with the peak ratio between the long-wavelength and short-wavelength (0.5–4 Å) channels (the ratio has a value of 14.75). We used these data and the formulation of Mewe et al. (1985) to derive a plasma temperature of 5.07 MK. The GOES data indicate that the maximum temperature range during the flare was 4.39–5.53 MK. These temperature estimates are consistent with results from the MESSENGER X-Ray Spectrometer, showing that the minimum temperature at which Ca XRF (which we do not detect in our XRF spectra) from Mercury's surface can be detected and distinguished from the scattered Ca X-ray background is ~8 MK (Nittler et al., 2011; Weider et al., 2012b). We therefore conducted our abundance modelling of the seven ROI spectra at assumed flare temperatures (for which we have atomdb spectra) of 4.0 MK (lower-limit),

5.0 MK (preferred value), and 6.3 MK (upper-limit). The atomdb modelled solar spectra for these three temperatures are shown in Figure 4.

3. Results

The fitted spectra for each ROI within the ground track are shown in Figure 2. These show the resolved low-energy K_α peaks of Mg, Al, and Si (the modelling also includes the adjacent K_β lines, but these are not resolved here). The relative variation in the strength of these lines is clear. The resultant Mg and Al abundances for the modelling at solar temperatures of 4.0 MK, 5.0 MK, and 6.3 MK are given in Table 2. We convert these results to provide equivalent MgO/SiO_2 and Al_2O_3/SiO_2 ratios because oxides are more commonly used in geochemical studies. The values we derive for a solar temperature of 5.0 MK are given in Table 3. The errors we quote in Table 3 represent the range exhibited from modelling at the other two solar temperatures (i.e., 4.0 and 6.3 MK), which take into account the uncertainty that arises from the absence of a direct solar spectrum measurement. The same ratios are illustrated in Figure 3a in context with lunar samples and Lunar Prospector gamma-ray spectroscopy data. Although a peak at ~1 keV (corresponding to Na K_α) can be seen in most of the spectra, the abundance results for Na are not reported because this line is likely to contain a contribution from scattered solar lines (as discussed by Weider et al., 2012a).

4. Discussion

4.1. Variation along the ground track

Figure 5a illustrates the compositional variation amongst the flare ROI. The MgO/SiO_2 ratios of ROI 1 and 2 are significantly lower than the other regions. The differences between the ROI are better illustrated when their FeO and TiO_2 compositions are also considered. The average FeO and TiO_2 abundances for each ROI are derived here from Clementine multispectral reflectance data using the algorithms of Gillis et al. (2004) and Gillis et al. (2003), respectively. The MgO, Al_2O_3, TiO_2, and FeO contents (all

normalised to the average lunar surface SiO_2 value of 44.93 wt %; Prettyman et al., 2006) for the seven ROI are shown in Figure 6, along with data for mare basalts and ferroan anorthosites (FAN) rock samples, average Apollo and Luna soil samples, and regolith breccia lunar meteorites. The combination of datasets in Figure 6 illustrates that the majority of the ground track consists of low-Ti basalts, albeit with Al_2O_3/SiO_2 ratios that are generally higher than the majority of the sample collection.

ROI 1 is the only region that is clearly distinct from the other low-Ti basalt regions. It has lower MgO/SiO_2, FeO/SiO_2, and TiO_2/SiO_2 ratios and thus appears to be more representative of feldspathic soils and rock types found in the lunar ferroan anorthosite suite (FAN). This region is almost completely made up of highland material, but in its southerly extent it also includes a small part of the mare basalt lava flows in Oceanus Procellarum (see Figure 1). The C1XS-Clementine major element composition for ROI 1 should reflect a mixture of these two lithologies. We made simple mixing calculations in order to investigate whether a mixture of FAN and mare basalt material can produce the composition of ROI 1. Figure 1 indicates that ROI 1 is >85% highlands (higher albedo, and lower FeO and TiO_2 content than the mare) and <15% (low-Ti) mare basalt. Our calculations show that in terms of MgO/SiO_2, TiO_2/SiO_2, and FeO/SiO_2 its composition is roughly consistent with a FAN-low-Ti basalt mixing trend in approximately the correct ratio. However, the same mixing proportion cannot account for the C1XS Al_2O_3/SiO_2 ratio we derive (Figure 5a).

The apparently low Al_2O_3/SiO_2 ratio for ROI 1 may represent a surficial enhancement (C1XS is most sensitive to the top ~100 μm of the surface) of mare material over the highlands region due to its transfer in crater ejecta, but this is not indicated by an increased FeO content (see Figure 1b and Table 3), and is unlikely on such a large spatial scale (e.g., Quaide and Oberbeck, 1975).

An alternative explanation for this apparently aberrant composition may be that it represents the earliest analysed part of the flare. The early stages of solar flares, when the temperature of the emitting plasma is rising, are periods dominated by multi-thermal

plasma regimes; later stages are characterised by more isothermal regimes (Garcia, 1994). More complicated solar modelling than we employed may therefore be required to accurately reproduce the incident X-ray spectrum. However, the GOES data (Figure 3) show that the period corresponding to the ROI 1 integration is during a relatively steady part of the flare, when the X-ray flux was relatively constant. It is, therefore, unlikely that inaccurate solar modelling (especially given that our errors incorporate a large range of solar temperatures) accounts for the low Al_2O_3/SiO_2 ratio of ROI 1. Indeed, Al_2O_3/SiO_2 determined by C1XS for the basaltic regions of the ground track are in broad agreement with expectations (see below). This gives us some confidence that the low ratio recorded for ROI 1 is unlikely to be an artefact of the calibration.

It is possible that our mixing calculations between FAN and basaltic compositions are too simple to explain the composition of ROI 1. Invoking alternative feldspathic lithologies, such as a troctolite (sample 12071) or an impact melt breccia component (either clast-rich or clast-poor, as in table A5.39 of Papike et al., 1998), instead of FAN also fails to reproduce the C1XS result. If norite is substituted for FAN, we find that a norite-low-Ti basalt mixture, in the ~85:15 ratio required, reproduces the Al_2O_3/SiO_2, FeO/SiO_2, and TiO_2/SiO_2 ratios of ROI 1, but gives an MgO/SiO_2 ratio that is too high. Three component mixing calculations, using known lunar lithologies, also cannot match the C1XS composition for ROI 1.

It appears that the feldspathic (*i.e.*, FAN, anorthositic Mg-suite) rock samples in the collection may not be representative (especially in their Al content) of the lunar feldspathic highlands region we sample in ROI 1. Lunar Prospector (L.P.) data (discussed further in section 4.3) for this region also have lower Al_2O_3/SiO_2 values than the FAN samples; they are generally intermediate between the FAN and mare basalt compositions (see Figure 5a). However, the Al content of the landing site bulk soils from feldspathic regions (*i.e.,* Apollo 16 and Luna 20) are lower than the FAN rock samples and the compositions of these soils are more consistent with that of ROI 1 (see Figure 6). It is likely that these bulk soil samples are more representative of the regolith's topmost

surface, to which the C1XS measurements are sensitive (*i.e.,* the top ~100 μm) than the whole rock samples. It is therefore possible that feldspathic highland soils from unsampled regions of the Moon could be a better match for the C1XS-derived Al_2O_3/SiO_2 ratio. Indeed, two lunar meteorite breccia samples (Calcalong Creek and MET 01210) thought to be from locations that were not sampled during the Apollo and Luna missions (*e.g.,* Hill and Boynton, 2003; Arai et al., 2010; Joy et al., 2010) have Mg and Al contents that are a reasonable match to the ROI 1 composition (although we do not specifically suggest that either meteorite was launched from the region we observed).

The similarity in the MgO/SiO_2 and Al_2O_3/SiO_2 ratios of ROI 1 and 2 (Figure 5a) is surprising given the vastly different highlands-mare proportions of their footprints. ROI 2 represents material with lower Mg concentrations than the other basaltic regions along the ground track. This could be evidence of lower olivine concentrations, if the olivine is forsteritic, at the edge of Oceanus Procellarum than the interior, which would support the findings of Lucey (2004). As illustrated in Figure 1a, ROI 2 also includes the youngest lava flow (Hiesinger et al., 2003) within the ground track. A decrease in Mg content, and an increase in Fe, could be expected if the magma source of the local lava flows evolved with time, although this cannot be confirmed without direct sampling. The similarity of ROI 1 and 2 could therefore be a coincidence of predominantly low-Al and high-Mg feldspathic (ROI 1), and low-Mg and high-Al basaltic (ROI 2) materials.

For all the regions, other than ROI 1, an almost entirely basaltic composition is expected. Minor highlands material contributions derived from crater ejecta would be indicated by Al_2O_3/SiO_2 ratios that are slightly higher than those of low-Ti basalts (as we see in Figure 6). The C1XS-Clementine compositions are consistent with soil and regolith breccia samples representative of the well-mixed uppermost lunar surface.

4.2. Comparison to previously published C1XS data

Figure 5b illustrates the C1XS Oceanus Procellarum results in the context of lunar sample data (as in Figure 5a) and in comparison to previously published C1XS results

from three flares: (i) 5th July 2009, with a ground track in the southern nearside highlands, close to the crater Tycho (Narendranath et al., 2011); (ii) 12th December 2008, with a ground track through Mare Serenitatis (Weider et al., 2012a); and (iii) 10th January 2009, with a ground track through Mare Insularum, Mare Cognitum, and Mare Nubium that includes the Apollo 14 landing site (Weider et al., 2012a). All the C1XS data from predominantly basaltic regions are clearly distinct from the southern nearside highlands data (Narendranath et al., 2011). As expected, the highlands regions have much higher Al abundances due to their dominantly anorthositic nature. However, as noted by Narendranath et al. (2011), these results are unexpectedly Al-rich compared to samples of lunar feldspathic regoliths (Haskin and Warren, 1991; McKay et al., 1991).

Within error, C1XS results from all the basaltic regions have self-consistent MgO/SiO_2 and Al_2O_3/SiO_2 ratios. One of the objectives for C1XS was to map global variations in mare basalt deposits (Crawford et al., 2009), but Figure 5b (see also Figure 1a in Weider et al., 2012a) shows that the limited C1XS data are insufficient to meet this aim. Although mare basalts can differ widely in their major element composition, especially in terms of TiO_2, the errors on the C1XS Mg and Al data are too large to see any of this variation. The size of these errors is largely due to uncertainty in the knowledge of the incident solar spectrum. This, in turn, is due to the weak nature of the flares that have been analysed, with magnitudes below that from which C1XS was designed to obtain data.

4.3. Comparison to Lunar Prospector gamma-ray data

The MgO/SiO_2 and Al_2O_3/SiO_2 ratios for L.P. pixels that overlap with the C1XS ground track are given in Table 3 and displayed for comparison to the C1XS data in Figure 5a. The L.P. data points are coloured to match the C1XS ROI with which they overlap. The Al_2O_3/SiO_2 ratios from the two datasets are generally in good agreement, although the C1XS-derived value for ROI 1 is somewhat lower than the L.P. value (see section 4.1), and the C1XS value for ROI 5 is higher than the L.P. equivalent. The MgO/SiO_2 values from both datasets also tend to agree well, except for ROI 1 and 2 that have significantly

lower C1XS-Mg contents (the ROI 5 C1XS value is also slightly higher than the L.P value, but they agree within error).

The lack of agreement between C1XS and L.P. results, where it occurs, may be partly due to the incomplete overlap of the two sets of footprints, *i.e.*, the smaller C1XS footprints do not always encompass the full compositional variations observed by L.P. (Figure 1). Inconsistencies between planetary XRF and GRS datasets have been noted previously and it has been suggested (*e.g.,* Riner et al., 2008; Lim and Nittler, 2009; Narendranath et al., 2011; Weider et al., 2012a) that the two techniques sample chemically distinct parts of the regolith due to the different penetration depths of the incident solar X-rays (~100 μm) and the galactic cosmic rays (tens of centimetres) that stimulate gamma-ray emission. Our C1XS and L.P. results, however, do not consistently agree or disagree, and it is only for ROI 1 that the disagreement is significant for both MgO and Al_2O_3. We therefore find no evidence for a fundamental discrepancy between the two datasets. Indeed, GRS and XRS results for several major elements (*e.g.,* Al, S, Ca) on Mercury are in agreement (Nittler et al., 2011; Weider et al., 2012b; Peplowski et al., 2012; Evans et al., 2012). It is also possible that the L.P. Prettyman et al. (2006) abundances of Mg and Al (especially the former) are locally overestimated by up to ~5 wt% (Wöhler et al., 2011) and may explain at least part of the offset in Mg/Si seen in Figure 5a for the low-Mg regions (i.e., ROI 1 and 2).

5. Conclusions

XRF spectra obtained by C1XS on Chandrayaan-1 for a ground track through the western part of Oceanus Procellarum have been analysed in this paper and estimates of the MgO/SiO_2 and Al_2O_3/SiO_2 for seven individual footprints were provided. Together with the two flares presented in Weider et al. (2012a), these analyses represent all the basaltic regions sampled by C1XS and, therefore, provide a limited opportunity to investigate the major element diversity of mare basalts across the lunar surface.

Although Oceanus Procellarum consists of a mosaic of temporally and compositionally diverse lava flow units, the regions sampled within the C1XS flare ground track do not encompass this full range of diversity (*i.e.,* in TiO_2 content). Small variations in the C1XS footprints are better revealed when the C1XS-derived Mg and Al abundances are combined with Fe and Ti contents derived from Clementine multispectral reflectance data. Low-Ti basalts comprise the majority of the ground track, with the derived compositions generally falling within the range of returned mare basalt samples. We find a low-Mg region at the edge of the mare deposit, which supports previous reports of lower olivine contents in this area and may be evidence of local magma sources evolving with time.

One ROI at the northern end of the ground track, which incorporates highlands and a small amount of basaltic material, has a low Al_2O_3/SiO_2 ratio and a composition that cannot be reproduced by simple mixing of returned highland and mare basalt rock sample compositions. Feldspathic regolith samples are more consistent with the composition we derived for the highlands region, but inconsistencies between the C1XS results and the composition of known lunar samples illustrates the problem with comparing global remote sensing datasets to a limited number of samples from relatively small, and globally unrepresentative, regions of the Moon. This highlights the need for additional materials to be returned to Earth for analysis from carefully selected places on the lunar surface (*e.g.*, NRC, 2007; Crawford et al., 2012).

6. Acknowledgements

The authors thank Lucy Lim and three anonymous reviewers for helpful and insightful comments and suggestions on previous versions of this manuscript, and Oded Aharonson for careful editorial handling. We thank ESA and ISRO, as well as co-PIs M. Grande and P. Sreekumar, and the rest of the C1XS Science Team for support in mission planning, spacecraft operations, and data processing and archiving for C1XS on Chandryaan-1. S.Z.W., I.A.C., and K.H.J. acknowledge STFC and the Leverhulme Trust for financial support.

7. References

Alha, L., Huovelin, J., Nygård, K., Andersson, H., Esko, E., Howe, C.J., Kellett, B.J., Narendranath, S., Maddison, B.J., Crawford, I.A., Grande, M., Sreekumar, P., 2009. Ground calibration of the Chandrayaan-1 X-ray Solar Monitor (XSM). Nucl. Instrum. Methods Phys. Res. A 607, 544–553.

Arai, T., Hawke, B.R., Giguere, T.A., Misawa, K., Miyamoto, M., Kojima, H., 2010. Antarctic lunar meteorites Yamato-793169, Asuka-881757, MIL 05035, and MET 01210 (YAMM): Launch pairing and possible cryptomare origin. Geochim. Cosmochim. Acta 74, 2231–2248.

Bhandari, N., 2005. Chandrayaan-1: science goals. J. Earth Syst. Sci. 114, 701–709.

Blewett, D.T., Lucey, P.G., Hawke, B.R., Jolliff, B.L., 1997. Clementine images of lunar sample-return stations: refinement of FeO and TiO_2 mapping techniques. J. Geophys. Res. 102, 16319–16325.

Charette, M.P., McCord, T.B., Pieters, C., Adams, J.B., 1974. Application of remote spectral reflectance measurements to lunar geology classification and determination of titanium content of lunar soils. J. Geophys. Res. 79, 1605–1613.

Clark, P.E., Trombka, J.I., 1997. Remote X-ray spectrometry for NEAR and future missions: modeling and analyzing X-ray production from source to surface. J. Geophys. Res. 102, 16361–16384.

Crawford, I.A., Joy, K.H., Kellett, B.J., Grande, M., Anand, M., Bhandari, N., Cook, A.C., d'Uston, L., Fernandes, V.A., Gasnault, O., Goswami, J., Howe, C.J., Huovelin, J., Koschny, D., Lawrence, D.J., Maddison, B.J., Maurice, S., Narendranath, S., Pieters, C., Okada, T., Rothery, D.A., Russell, S.S., Sreekumar, P., Swinyard, B., Wieczorek, M.,

Wilding, M., 2009. The scientific rationale for the C1XS X-ray Spectrometer on India's Chandrayaan-1 mission to the Moon. Planet. Space Sci. 57, 725–734.

Crawford, I.A., Anand, M., Cockell, C.S., Falcke, H., Green, D.A., Jaumann, R., Wieczorek, M. A., 2012. Back to the Moon: The scientific rationale for resuming lunar surface exploration. Planet. Space Sci. 74, 3-14.

Davis, P.A., Jr., 1980. Iron and titanium distribution on the Moon from orbital gamma ray spectrometry with implications for crustal evolutionary models. J. Geophys. Res. 85 (B6), 3209–3224.

Elphic, R.C., Lawrence, D.J., Feldman, W.C., Barraclough, B.L., Gasnault, O.M., Maurice, S., Lucey, P.G., Blewett, D.T., Binder, A.B., 2002. Lunar Prospector neutron spectrometer constraints on TiO_2. J. Geophys. Res. 107 (E4), 5024, doi: 10.1029/2000JE001460.

Elphic, R.C., Lawrence, D.J., Feldman, W.C., Barraclough, B.L., Maurice, S., Binder, A.B., Lucey, P.G., 2000. Lunar rare earth element distribution and ramifications for FeO and TiO_2: Lunar Prospector neutron spectrometer observations. J. Geophys. Res. 105 (E8), 20333–20345.

Evans, L.G., Peplowski, P.N., Rhodes, E.A., Lawrence, D.J., McCoy, T.J., Nittler, L.R., Solomon, S.C., Sprague, A.L., Stockstill-Cahill, K.R., Starr, R.D., Weider, S.Z., Boynton, W.V., Hamara, D.K., Goldsten, J.O., 2012. Major-element abundances on the surface of Mercury: Results from the MESSENGER Gamma-Ray Spectrometer. J. Geophys. Res. 117, E00L07, doi: 10.1029/2012JE004178.

Fruland, R.M., 1983. Regolith Breccia Workbook, JSC 19045. NASA Johnson Space Center, Houston.

Garcia, H.A., 1994. Temperature and emission measure from GOES soft X-ray measurements. Sol. Phys. 154, 275–308.

Giguere, T.A., Taylor, G.J., Hawke, B.R., Lucey, P.G., 2000. The titanium contents of lunar mare basalts. Meteorit. Planet. Sci. 35, 193–200.

Gillis, J.J., Jolliff, B.L., Elphic, R.C., 2003. A revised algorithm for calculating TiO_2 from Clementine UVVIS data: a synthesis of rock, soil, and remotely sensed TiO_2 concentrations. J. Geophs. Res. 108 (E2), 5009, doi: 10.1029/2001JE001515.

Gillis, J.J., Jolliff, B.L., Korotev, R.L., 2004. Lunar surface geochemistry: global concentrations of Th, K, and FeO as derived from Lunar Prospector and Clementine data. Geochim. Cosmochim. Acta 68, 3791–3805.

Goswami, J.N., Annadurai, M., 2009. Chandrayaan-1: India's first planetary science mission to the moon. Curr. Sci. 96, 486–491.

Grande, M., Maddison, B.J., Howe, C.J., Kellett, B.J., Sreekumar, P., Huovelin, J., Crawford, I.A., d'Uston, C.L., Smith, D., Anand, M., Bhandari, N., Cook, A., Fernandes, V., Foing, B., Gasnault, O., Goswami, J.N., Holland, A., Joy, K.H., Kochney, D., Lawrence, D., Maurice, S., Okada, T., Narendranath, S., Pieters, C., Rothery, D., Russell, S.S., Shrivastava, A., Swinyard, B., Wilding, M., Wieczorek, M., 2009a. The C1XS X-ray Spectrometer on Chandrayaan-1. Planet. Space Sci. 57, 717–724.

Grande, M., Maddison, B.J., Sreekumar, P., Huovelin, J., Kellett, B.J., Howe, C.J., Crawford, I.A., Smith, D.R., the C1XS Team, 2009b. The Chandrayaan-1 X-ray Spectrometer. Curr. Sci. 96, 517–519.

Hackwill, T., Guest, J., Spudis, P., 2006. Stratigraphy and evolution of basalts in Mare Humorum and southeastern Procellarum. Meteorit. Planet. Sci. 41, 479–488.

Haskin, L., Warren, P., 1991. Lunar chemistry. In: Heiken, G.H., Vaniman, D.T., French, B.M. (Eds.) Lunar Sourcebook: a user's guide to the moon. Cambridge University Press, 357–474.

He, F., Van Espen, P.J., 1991. General approach for quantitative energy dispersive X-ray fluorescence analysis based on fundamental parameters. Anal. Chem. 63, 2237–2244.

Hiesinger, H., Head, J.W., III, Wolf, U., Jaumann, R., Neukum, G., 2003. Ages and stratigraphy of mare basalts in Oceanus Procellarum, Mare Nubium, Mare Cognitum, and Mare Insularum. J. Geophys. Res. 108 (E7), 5065, doi: 10.1029/2002JE001985.

Hiesinger, J., Head, J.W., III, Wolf, U., Jaumann, R., Neukum, G., 2011. Ages and stratigraphy of lunar mare basalts: a synthesis. Geol. Soc. Am. Spec. Pap. 477, 1–51.

Hill, D.H., Boynton, W.V., 2003. Chemistry of the Calcalong Creek lunar meteorite and its relationship to lunar terranes. Meteorit. Planet. Sci. 38, 595–626.

Howe, C.J., Drummond, D., Edeson, R., Maddison, B., Parker, D.J., Parker, R., Shrivastaa, A., Spencer, J., Kellett, B.J., Grande, M., Sreekumar, P., Huovelin, J., Smith, D.R., Gow, J., Narendranath, S., d'Uston, L., 2009. Chandrayaan-1 X-ray Spectrometer (C1XS) – Instrument design and technical details. Planet. Space Sci. 57, 735–743.

Huovelin, J., Alha, L., Andersson, H., Andersson, T., Browning, R., Drummond, D., Foing, B., Grande, M., Hämäläinen, K., Laukkanen, J., Lämsä, V., Muinonen, K., Murray, M., Nenonen, S., Salminen, A., Sipilä, H., Taylor, L., Vilhu, O., Waltham, N., Lopez-Jorkama, M., 2002. The SMART-1 X-ray solar monitor (XSM): calibrations for D-CIXS and independent coronal science. Planet. Space Sci. 50, 1345–1353.

Jerde, E.A., Morris, R.v., Warren, P.H., 1990. In quest of lunar regolith breccias of exotic provenance: a uniquely anorthositic sample from the Fra Mauro (Apollo 14) highlands. Earth Planet. Sci. Lett. 98, 90–108.

Jerde, E.A., Warren, P.H., Morris, R.V., Heiken G.H., Vaniman, D.T., 1987. A potpurri of regolith breccias: "new" samples from the Apollo 14, 16 and 17 landing sites. Proc. Lunar Planet. Sci. Conf., J. Geophys. Res. 92 (B4), E526–E536.

Johnson, J.R., Larson, S.M., Singer, R.B., 1991. Remote sensing of potential lunar resources 1. near-side compositional properties. J. Geophys. Res. 96 (E3), 18861–18882.

Joy, K.H., Crawford, K.H., Russell, S.S., Kearsley, A.T., 2010. Lunar meteorite regolith breccias: An in situ study of impact melt composition using LA-ICP-MS with implications for the composition of the lunar crust. Meteorit. Planet. Sci. 45, 917–946.

Korotev, R.L., 2012. Lunar meteorites from Oman. Meteorit. Planet. Sci. 47, 1365–1402.

Lim, L.F., Nittler, L.R., 2009. Elemental composition of 433 Eros: new calibration of the NEAR-Shoemaker XRS data. Icarus 200, 129–146.

Lucey, P.G., 2004. Mineral maps of the Moon. Geophys. Res. Lett. 31, L08701, doi: 10.1029/2003GL019406.

Maruyama, Y., Ogawa, K., Okada, T., Kato, M., 2008. Laboratory experiments of particle size effect in X-ray fluorescence and implications to remote X-ray spectrometry of lunar regolith surface. Earth Planets Space 60, 293–297.

McKay, D.S., Bogard, D.D., Morris, R.V., Korotev, R.L., Johnson, P. Wentworth, S.J., 1986. Apollo 16 regolith breccias: characterization and evidence for early formation in the mega-regolith. Proc Lunar Planet. Sci. Conf. XVI, J. Geophys. Res. 91 (B4), D277–D303.

McKay, D.S., Bogard, D.D., Morris, R.V., Korotev, R.L., Wentworth, S.J., Johnson, P., 1989. Apollo 15 regolith breccias: window to a KREEP regolith. Proc. Lunar Planet. Sci. Conf. IXX, 19–41.

McKay, D.S., Heiken, G., Basu, A., Blanford, G., Simon, S., Reedy, R., French, B.M., Papike, J., 1991. The lunar regolith. In: Heiken, G.H., Vaniman, D.T., French, B.M. (Eds.) Lunar Sourcebook: a user's guide to the moon. Cambridge University Press, 285–356.

Mewe, R., Gronenschild, E.H.B.M., van den Oord, G.H.J., 1985. Calculated X-radiation from optically thin plasma. V. Astron. Astrophys. Suppl. Ser. 62, 197–254.

Morris, R.V., Score, R., Dardano, C., Heiken, G., 1983. Handbook of Lunar Soils, JSC 19069. NASA Johnson Space Center, Houston.

Näränen, J., Parviainen, H., Muinonen, K., Carpenter, J., Nygård, K., Peura, M., 2008. Laboratory studies into the effect of regolith on planetary X-ray fluorescence spectroscopy. Icarus 198, 408–419.

Narendranath, S., Sreekumar, P., Maddison, B.J., Howe, C.J., Kellett, B.J., Wallner, M., Erd, C., Weider, S.Z., 2010. Calibration of the C1XS instrument on Chandrayaan-1. Nucl. Instrum. Methods Phys. Res. A 621, 344–353.

Narendranath, S., Athiray, P.S., Sreekumar, P., Kellett, B.J., Alha, L., Howe, C.J., Joy, K.H., Grande, M., Huovelin, J., Crawford, I.A., Unnikrishnan, U., Lalita, S., Subramaniam, S., Weider, S.Z., Nittler, L.R., Gasnault, O., Rothery, D., Fernandes, V.A., Bhandari, N., Goswami, J.N., Wieczorek, M.A., the C1XS team, 2011. Lunar X-ray fluorescence observations by the Chandrayaan-1 X-ray Spectrometer (C1XS): results from the nearside southern highlands. Icarus 214, 53–66.

Neal, C.R., Taylor, L.A., 1992. Petrogenesis of mare basalts: a record of lunar volcanism. Geochim. Cosmochim. Acta 56, 2177–2211.

Nittler, L.R., Starr, R.D., Weider, S.Z., McCoy, T.J., Boynton, W.V., Ebel, D.S., Ernst, C.M., Evans, L.G., Goldsten, J.O., Hamara, D.K., Lawerence, D.J., McNutt, R.L., Jr., Schlemm, C.E., II, Solomon, S.C., Sprague, A.L., 2011. The major-element composition of Mercury's surface from MESSENGER X-ray spectrometry. Science 333, 1847–1850.

NRC, 2007. The Scientific Context for Exploration of the Moon. National Research Council, Washington, DC. http://www.nap.edu/catalog.php?record_id=11954.

Papike, J.J., Ryder, G., Shearer, C.K., 1998. Lunar samples. Rev. Miner. 36, 5.1–5.234.

Parviainen, H., Näränen, J., Muinonen, K., 2011. Soft X-ray fluorescence from particulate media: Numerical simulations. J. Quant. Spectrosc. Radiat. Transf. 112, 1907–1918.

Peplowski, P.N., Rhodes, E.A., Hamara, D.K., Lawrence, D.J., Evans, L.G., Nittler, L.R., Solomon, S.C., 2012. Aluminum abundance on the surface of Mercury: Application of a new background reduction technique for the analysis of gamma-ray spectroscopy data. J. Geophys. Res. 117, E00L10, doi: 10.1029/2012JE004181.

Pieters, C.M., 1978. Mare basalt types on the front side of the moon: a summary of spectral reflectance data. Proc. Lunar Planet. Sci. Conf. IX, 2825–2849.

Pieters, C.M., Head, J.W., Adams, J.B., 1980. Late high-titanium basalts of the western maria: geology of the Flamsteed region of Oceanus Procellarum. J. Geophys. Res. 85 (B7), 3913–3938.

Prettyman, T.H., Hagerty, J.J., Elphic, R., Feldman, W.C., Lawrence, D.J., McKinney, G.W., Vaniman, D.T., 2006. Elemental composition of the lunar surface: analysis of

gamma ray spectroscopy data from Lunar Prospector. J. Geophys. Res. 111, E12007, doi: 10.1029/2005JE002656.

Quaide, W., Oberbeck, V., 1975. Development of the mare regolith: Some model considerations. The Moon 13, 27–55.

Rhodes, J.M., Blanchard, D.P., 1981. Apollo 11 breccias and soils: aluminous mare basalts or multi-component mixtures? Proc. Lunar Planet. Sci. Conf XII, 607–620.

Riner, M.A., Robinson, M.S.,Eckart, J.M., Desch., S.J., 2008. Global survey of color variations on 433 Eros: implications for regolith processes and asteroid environments. Icarus 198, 67–76.

Simon, S.B., Papike, J.J., Gosselin, D.C., Laul, J.C., 1985. Petrology and chemistry of Apollo 12 regolith breccias. Proc. Lunar Planet. Sci. Conf. XVI, J. Geophys. Res. 90, D75–D86.

Staid, M.I., Pieters, C.M., Besse, S., Boardman, J., Dhingra, D., Green, R., Head, J.W., Isaacson, P., Klima, R., Kramer, G., Mustard, J.M., Runyon, C., Sunshine, J., Taylor, L.A., 2011. The mineralogy of late stage lunar volcanism as observed by the Moon Mineralogy Mapper on Chandrayaan-1. J. Geophys. Res. 116, E00G10, doi: 10.1029/2010JE003735.

Swinyard, B.M., Joy, K.H., Kellett, B.J., Crawford, I.A., Grande, M., Howe, C.J., Fernandes, V.A., Gasnault, O., Lawrence, D.J., Russell, S.S., Wieczorek, M.A., Foing, B.H., The SMART-1 team, 2009. X-ray fluorescence observations of the Moon by SMART-1/D-CIXS and the first dection of Ti Kα from the lunar surface. Planet. Space Sci. 57, 744–750.

Weider, S.Z., Kellett, B.J., Swinyard, B.M., Crawford, I.A., Joy, K.H., Grande, M., Howe, C.J., Huovelin, J., Narendranath, S., Alha, L., Anand, M., Athiray, P.S., Bhandari,

N., Carter, J.A., Cook, A.C., d'Uston, L.C., Fernandes, V.A. Gasnault, O., Goswami, J.N., Gow, J.P.D., Holland, A.D., Koschny, D., Lawrence, D.J., Maddison, B.J., Maurice, S., McKay, D.J., Okada, T., Pieters, C., Rothery, D.A., Russell, S.S., Shrivastava, A., Smith, D.R., Wieczorek, M., 2012a. The Chandrayaan-1 X-ray Spectrometer: first results. Planet. Space Sci. 60, 217–228.

Weider, S.Z., Nittler, L.R. ,Starr, R.D., McCoy, T.J., Stockstill-Cahill, K.R., Byrne, P.K., Denevi, B.W., Head, J.W., Solomon, S.C., 2012b. Chemical heterogeneity on Mercury's surface revealed by the MESSENGER X-ray spectrometer. J. Geophys. Res. 117, E00L05, doi:10.1029/2012JE004153.

Weider, S.Z., Swinyard, B.M., Kellett, B.J., Howe, C.J., Joy, K.H., Crawford, I.A., Gow, J., Smith, D.R., 2011. Planetary X-ray fluorescence analogue laboratory experiments and an elemental abundance algorithm for C1XS. Planet. Space Sci. 59, 1393–1407.

Wieczorek, M.A., Jolliff, B.L., Khan, A., Pritchard, M.E., Weiss, B.P., Williams, J.G., Hood, L.L., Righter, K., Neal, C.R., Shearer, C.K., McCallum, I.S., Tompkins, S., Hawke, B.R., Peterson, C., Gillis, J.J., Bussey, B., 2006. The constitution and structure of the lunar interior. Rev. Mineral. Geochem. 60, 221–364.

Wilhelms, D.E., McCauley, J.F., Trask, N.J., 1987. The Geologic History of the moon. U.S. Geological Survey, Washington D.C.

Wöhler, C., Berezhnoy, A., Evans, R., 2011. Estimation of elemental abundances of the lunar regolith using Clementine UVVIS+NIR data. Planet. Space Sci. 59, 92–110.

Yin, L.I., Trombka, J.I., Adler, I., Bielefeld, M., 1993. X-ray remote sensing techniques for geochemical analysis of planetary surfaces. In: Pieters, C.M., Englert, P.A.J. (Eds.) Remote geochemical analysis, elemental and mineralogical composition. Cambridge University Press, 199–212.

Table 1. Boresight location and phase angle for each of the regions of interest in the C1XS Oceanus Procellarum observation.

	Start				End			
ROI	**Time (U.T.)**	**Boresight longitude (°)**	**Boresight latitude (°)**	**Phase angle (°)**	**Time (U.T.)**	**Boresight longitude (°)**	**Boresight latitude (°)**	**Phase angle (°)**
1	23:07:23	-69.24	66.88	76.93	23:10:59	-69.34	55.99	71.47
2	23:11:21	-69.35	54.88	70.94	23:13:45	-69.39	47.61	67.63
3	23:13:45	-69.39	47.61	67.63	23:17:20	-69.45	36.75	63.26
4	23:17:42	-69.46	35.64	62.87	23:20:30	-69.50	27.15	60.15
5	23:20:53	-69.50	25.98	59.83	23:21:42	-69.52	23.50	59.18
6	23:22:04	-69.52	22.39	58.91	23:24:04	-69.55	16.31	57.66
7	23:24:38	-69.55	14.59	57.38	23:26:03	-69.57	10.28	56.81

Table 2. Modelled abundances (elemental wt%) for Mg and Al, from each of the Oceanus Procellarum ROI spectra, with 1 σ fitting errors provided. Values are given for the best estimate of the flare temperature (5.0 MK; million Kelvin) and the upper and lower temperature estimates (4.0 MK and 6.3 MK). The O and Si values are fixed in the modelling at the Lunar Prospector (Prettyman et al., 2006) average lunar surface composition values of 44.00 and 21.00 element wt %, respectively.

	4.0 MK		5.0 MK		6.3 MK	
ROI	**Mg**	**Al**	**Mg**	**Al**	**Mg**	**Al**
1	2.25 ± 0.50	7.75 ± 1.00	3.00 ± 0.63	9.25 ± 1.13	4.25 ± 1.00	10.50 ± 1.38
2	2.75 ± 0.38	8.00 ± 0.63	3.50 ± 0.50	9.25 ± 0.63	4.75 ± 0.75	10.75 ± 0.75
3	5.75 ± 0.38	7.75 ± 0.88	7.75 ± 0.50	9.25 ± 1.00	10.25 ± 0.75	10.50 ± 1.25
4	4.25 ± 0.25	7.50 ± 0.50	5.75 ± 0.25	8.75 ± 0.63	7.50 ± 0.38	10.25 ± 0.88
5	5.75 ± 0.50	9.75 ± 0.88	7.75 ± 0.75	11.50 ± 1.13	10.25 ± 1.00	13.25 ± 1.25
6	4.00 ± 0.25	8.25 ± 0.63	5.25 ± 0.38	9.75 ± 0.63	7.00 ± 0.63	11.00 ± 0.75
7	4.50 ± 0.38	9.50 ± 0.75	6.00 ± 0.50	11.50 ± 0.88	8.00 ± 0.75	13.00 ± 1.00

Table 3. C1XS MgO/SiO_2 and Al_2O_3/SiO_2 ratios for the seven regions of interest (ROI) within the Oceanus Procellarum flare. These values are derived from modelling of the spectra at the best temperature estimate of 5.0 MK (see Table 2). The errors represent the range exhibited from modelling at the lower and upper temperature estimates (4.0 and 6.3 MK). The C1XS values are compared to the Lunar Prospector (L.P.) gamma-ray results (Prettyman et al., 2006) for pixels (whose index values are provided in parenthesis next to the L.P. MgO/SiO_2 values) that overlap with the C1XS regions (as shown in Figure 1). The mean L.P. ratios for each ROI are calculated from the individual values of the relevant pixels. The errors given for the mean L.P. values are the standard deviation of the individual values. The Clementine derived TiO_2/SiO_2 and FeO/SiO_2 values (errors quoted are for 1 elemental wt % Ti or Fe) for each ROI are also given, as shown in Figure 5 and Figure 6.

ROI	**MgO/SiO_2**			**Al_2O_3/SiO_2**			**TiO_2/SiO_2**	**FeO/SiO_2**
	C1XS	**L.P.**	**L.P. mean**	**C1XS**	**L.P.**	**L.P. mean**		
1	0.11 +0.05/-0.03	0.23 ± 0.02 (1609) 0.20 ± 0.02 (1653) 0.21 ± 0.02 (1691) 0.20 ± 0.02 (1692)	0.21 ± 0.01	0.39 +0.05/-0.06	0.52 ± 0.03 0.51 ± 0.03 0.47 ± 0.02 0.67 ± 0.02	0.54 ± 0.09	0.01 ± 0.02	0.15 ± 0.02
2	0.13 +0.05/-0.03	0.22 ± 0.02 (1562) 0.23 ± 0.02 (1609)	0.23 ± 0.01	0.39 +0.06/-0.05	0.35 ± 0.03 0.52 ± 0.03	0.44 ± 0.09	0.04 ± 0.02	0.34 ± 0.02
3	0.29 +0.09/-0.07	0.27 ± 0.02 (1386) 0.29 ± 0.02 (1446) 0.24 ± 0.02 (1506) 0.22 ± 0.02 (1562)	0.27 ± 0.03	0.39 +0.05/-0.06	0.38 ± 0.03 0.44 ± 0.03 0.39 ± 0.03 0.35 ± 0.03	0.39 ± 0.03	0.05 ± 0.02	0.41 ± 0.02
4	0.21 +0.07/-0.06	0.21 ± 0.03 (1245) 0.23 ± 0.03 (1246) 0.23 ± 0.03 (1317) 0.30 ± 0.03 (1318) 0.27 ± 0.02 (1386)	0.25 ± 0.04	0.37 +0.06/-0.05	0.36 ± 0.03 0.27 ± 0.03 0.34 ± 0.03 0.37 ± 0.03 0.38 ± 0.03	0.34 ± 0.04	0.07 ± 0.02	0.40 ± 0.02
5	0.29 +0.09/-0.07	0.21 ± 0.03 (1245) 0.23 ± 0.03 (1246)	0.22 ± 0.01	0.49 ± 0.07	0.36 ± 0.03 0.27 ± 0.03	0.32 ± 0.04	0.06 ± 0.02	0.39 ± 0.02
6	0.20 +0.07/-0.05	0.29 ± 0.03 (1101) 0.21 ± 0.02 (1102) 0.23 ± 0.03 (1173) 0.21 ± 0.03 (1174)	0.24 ± 0.04	0.41 +0.05/-0.06	0.31 ± 0.33 0.40 ± 0.03 0.30 ± 0.03 0.27 ± 0.03	0.32 ± 0.06	0.06 ± 0.02	0.44 ± 0.02
7	0.22 +0.07/-0.06	0.20 ± 0.03 (1029) 0.28 ± 0.03 (1030) 0.29 ± 0.03 (1101) 0.21 ± 0.02 (1102)	0.25 ± 0.05	0.49 +0.06/-0.08	0.56 ± 0.03 0.48 ± 0.03 0.31 ± 0.33 0.40 ± 0.03	0.44 ± 0.11	0.06 ± 0.02	0.38 ± 0.02

Figure 1. Maps (simple cylindrical projection) of (a) albedo, (b) FeO wt%, and (c) TiO_2 wt% for the region around the Oceanus Procellarum C1XS flare ground track. The abundances shown in (b) and (c) are derived using Clementine multispectral reflectance data according to the algorithms of Gillis et al. (2004) and (2003), respectively. Overlain on the albedo image in (a) is the lava flow mapping of Hiesinger et al. (2003) where units are coloured according to their estimated, crater-count age. The C1XS ground track (bold) is split into seven regions of interest (ROI), which are labelled; also shown are the boundaries (faint dotted lines) of the 5° Lunar Prospector gamma-ray dataset pixels (Prettyman et al., 2006) for the area overlapping with the C1XS ground track (Lunar Prospector index numbers are given to the right of the panels). The C1XS footprints have a full width of 50 km and range in length from 385 km for ROI 1 in the north to 185 km for ROI 7 in the south.

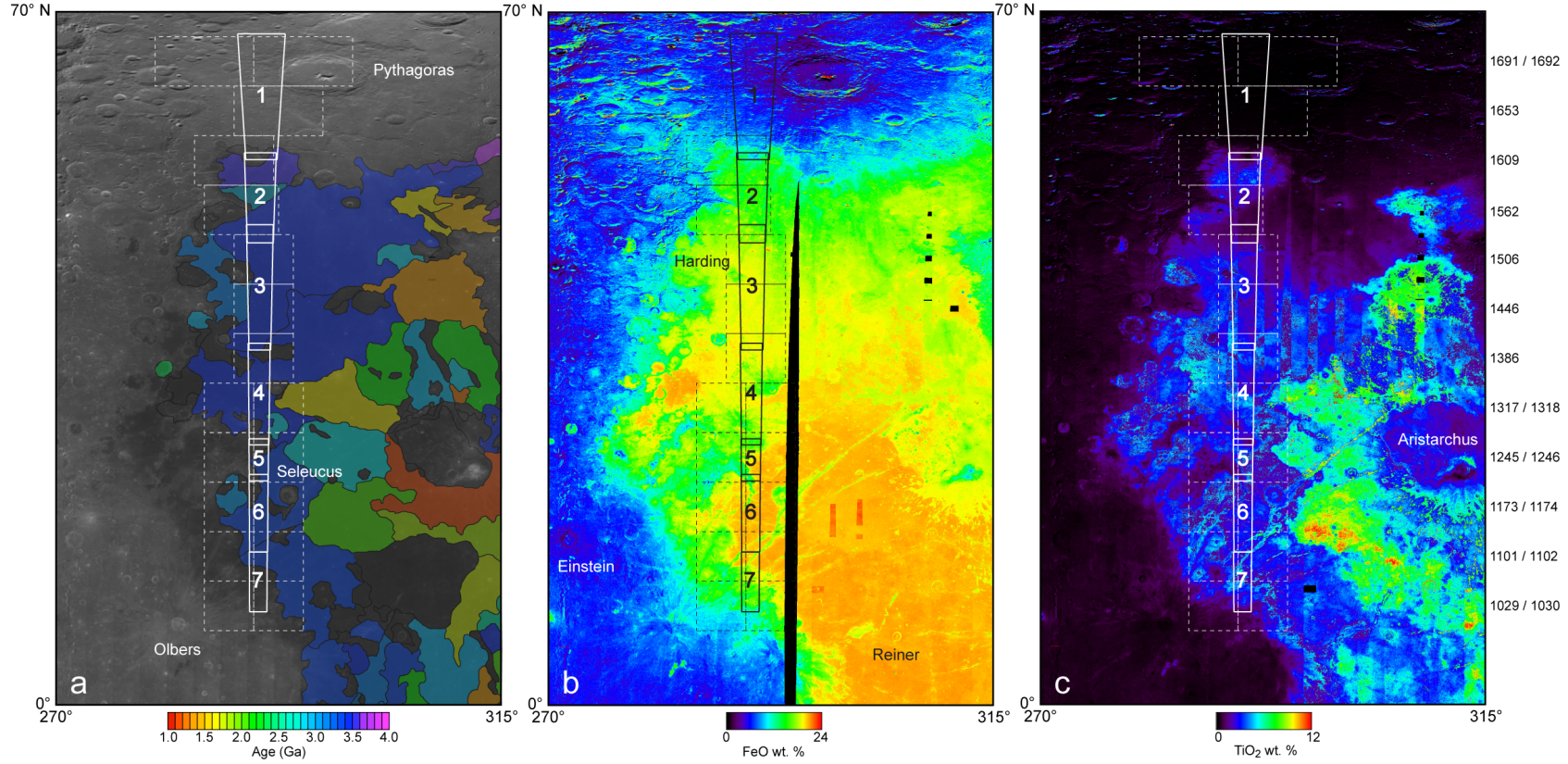

Figure 2. Background-subtracted C1XS spectra for each of the seven ROI within the Oceanus Procellarum flare ground track. The RAL abundance algorithm fitted model (generated using a 5.0 MK solar model) for each spectrum is also shown (smooth bold line), as well as the weighted residual in each case. The Mg K_α (1.25 keV), Al K_α (1.49 keV), and Si K_α (1.74 keV) peaks, which are labelled in (a), are clearly resolved in each case. The more indistinct peak at ~1 keV (in the spectra of ROI 3 - 7) may be partly due to Na K_α (1.04 keV), labelled in (d), but likely contains a significant contribution from scattered solar lines (this has been discussed previously by Weider et al., 2012); the apparent 'peak' below 1 keV is a data processing artefact caused by instrument noise. The weighted residual given in the lower panel for each spectrum is the residual of the fitting normalised to the standard deviation of the noise in the spectrum. This noise measure is taken from the continuum between 2.5 and 3.0 keV, and as such represents the native detector and photon shot noise close to the region of interest. Systematic effects dominate the residuals where they are high, and are reflected in the overall errors quoted on the abundance ratios.

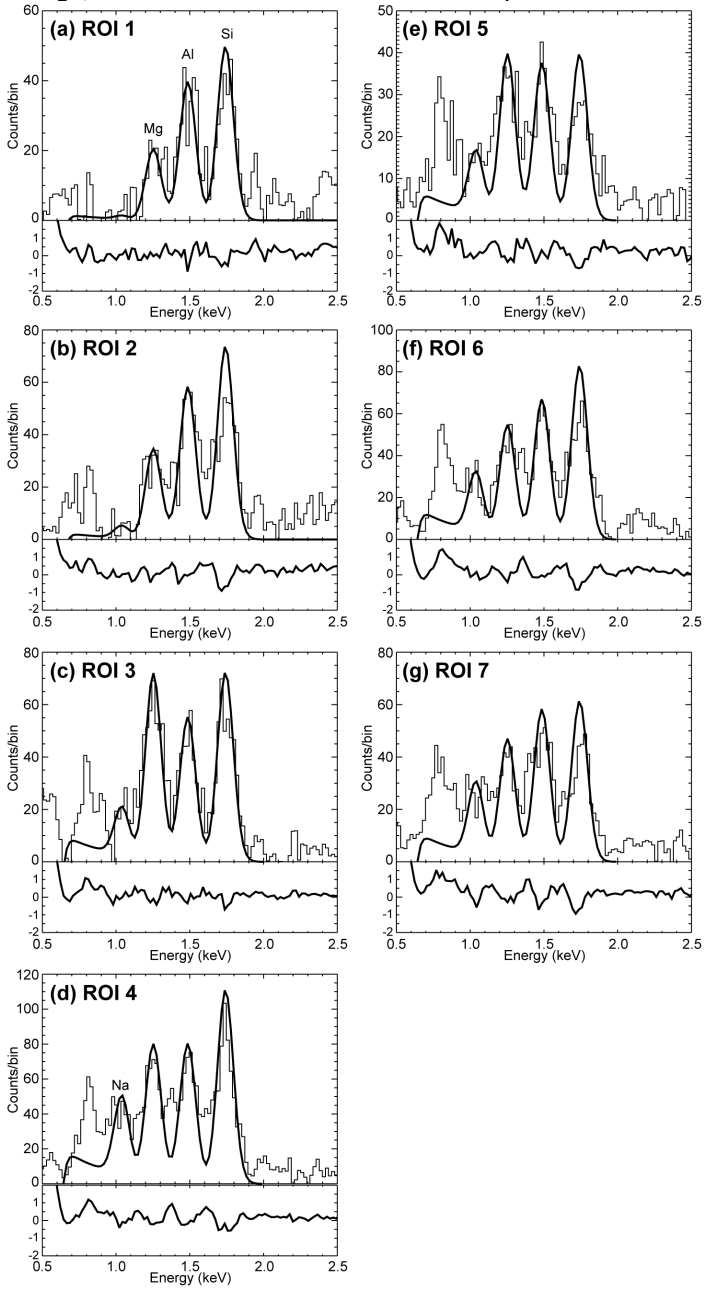

Figure 3. Geostationary Operational Environmental Satellite (GOES-10) X-ray flux data between 23:00 U.T. on 10th February 2009 and 00:40 U.T. on 11th February 2009. The start and end of the flare period analysis (see Table 1) are indicated by the dashed lines. Open symbols: Data from the long-wavelength channel (1–8 Å); closed symbols: Data from the short-wavelength channel (0.5–4 Å).

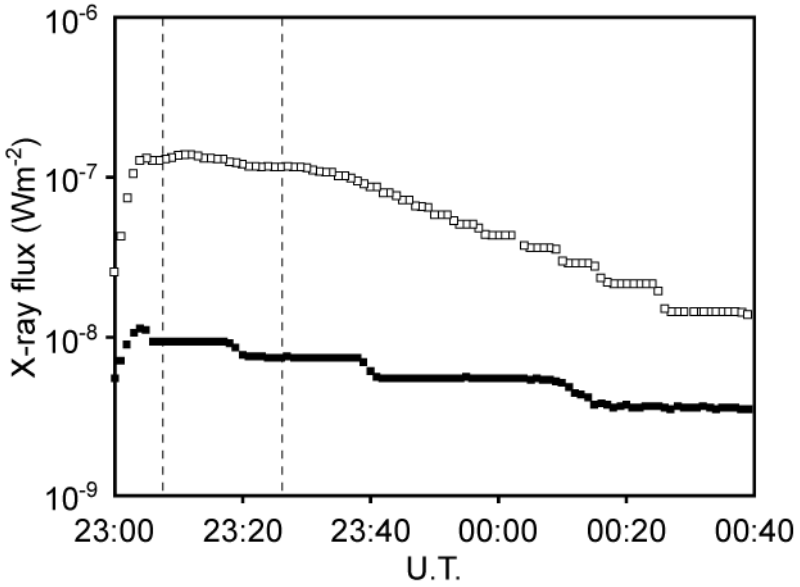

Figure 4. Modelled solar spectra from the *atomdb* (version 2.0.0) database and software. Spectra generated for the three different solar plasma temperatures, 4.0 MK (blue), 5.0 MK (green), and 6.3 MK (red), used in the C1XS forward modelling are shown in the 0.5–5 keV energy range.

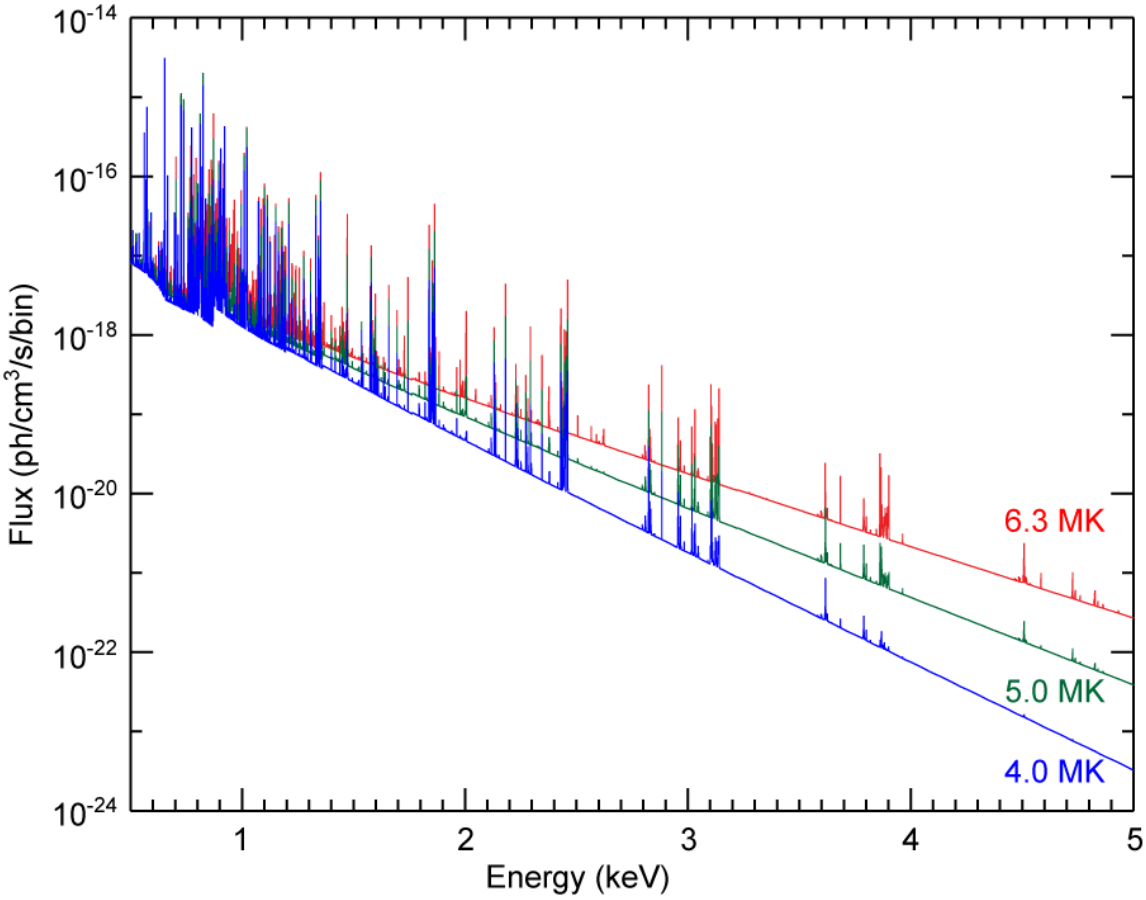

Figure 5. Plots of MgO/SiO_2 versus Al_2O_3/SiO_2 for the C1XS Oceanus Procellarum flare. In (a) the results (coloured diamonds, labelled with the ROI number) are compared to (i) Lunar Prospector (L.P.) gamma-ray data (Prettyman et al., 2006) for the pixels (see Figure 1 and Table 3) that overlap with the C1XS ROI (circles, coloured to match the appropriate C1XS ROI); (ii) the bulk (average) soil compositions from each of the Apollo and Luna returned sample landing sites (Haskin and Warren, 1991; McKay et al., 1991); (iii) sample compositions of various lunar lithologies: the mare basalts, ferroan anorthosites (FAN), Mg-suite and alkali-suite (data from Papike et al., 1998 and references therein, and from the Lunar Mare Basalt Database: http://www.nd.edu/~cneal/Lunar-L), whose general fields are labelled; and (iv) compositions for lunar meteorite breccias (data from Wieczorek et al., 2006; Joy et al., 2010; Korotev, 2012). The C1XS data points are plotted at the values generated from forward modelling at 5.0 MK; the error bars represent the range exhibited by modelling at the lower and upper temperature estimates of 4.0 MK and 6.3 MK (see Table 2). In (b) the C1XS Procellarum flare results (coloured diamonds) are compared to lunar sample compositions as in (a), as well as to previously published C1XS results from three other flares: (i) 12th December 2008, including its Mare Serenitatis (M.S.) section (Weider et al., 2012); (ii) 10th January 2009 (through Mare Insularum, Mare Cognitum and Mare Nubium), including its Fra Mauro Formation (F.M.) section (Weider et al., 2012); and (iii) 5th July 2009 through the nearside southern highlands (Narendranath et al., 2011).

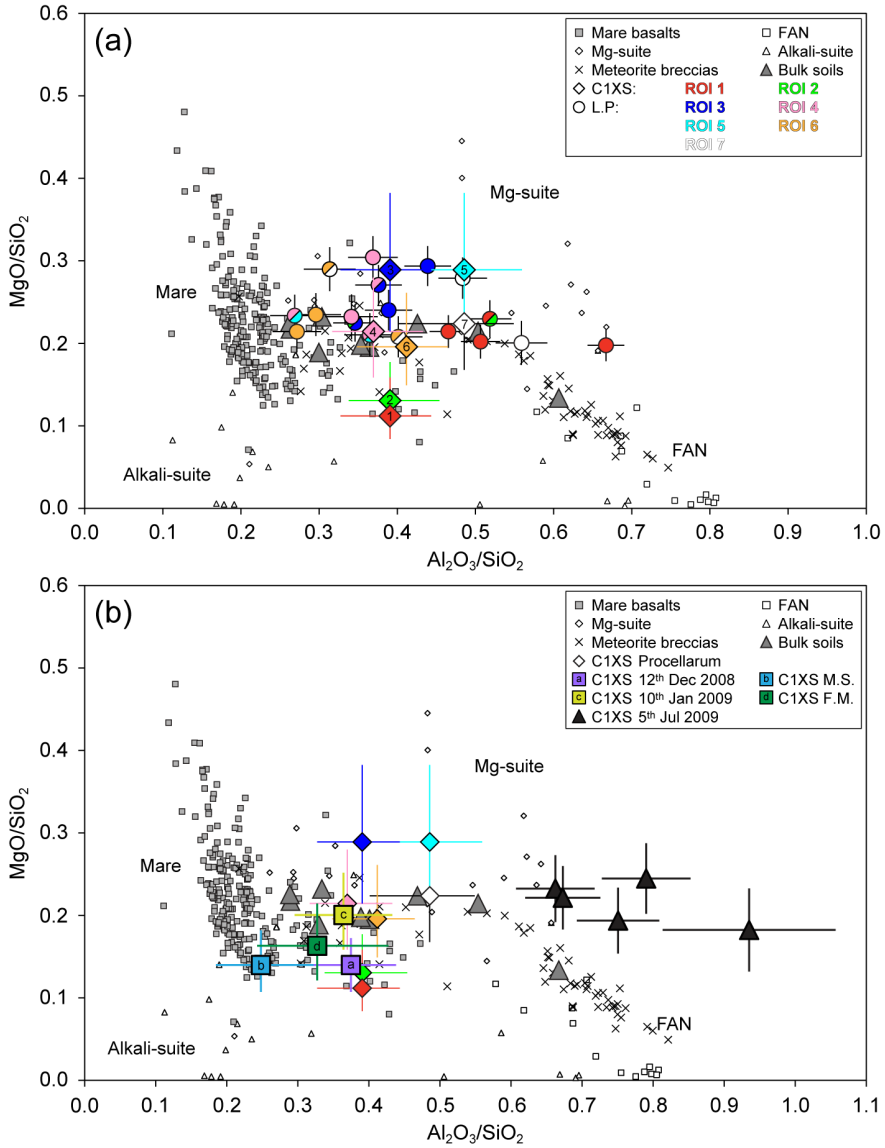

Figure 6. Compositions of the C1XS ROI: (a) TiO_2/SiO_2 versus MgO/SiO_2, (b) TiO_2/SiO_2 versus Al_2O_3/SiO_2, (c) FeO/SiO_2 versus MgO/SiO_2, and (d) FeO/SiO_2 versus Al_2O_3/SiO_2, where the MgO/SiO_2 and Al_2O_3/SiO_2 ratios are the C1XS results presented in this paper and the TiO_2/SiO_2 and FeO/SiO_2 ratios are derived from Clementine multispectral reflectance data, with 1 wt % error bars, according to the algorithms of Gillis et al. (2003) and Gillis et al. (2004), respectively (these algorithms return values for FeO and TiO_2, these have been normalised to the fixed SiO_2 value used in the C1XS modelling). These values are compared to the compositions of (i) mare basalts (categorized according to their Ti-content, following the classification scheme of Neal and Taylor, 1992); (ii) ferroan anorthosite (FAN) samples (data taken from Papike et al., 1998 and references therein); (iii) the bulk (average) soils from each of the Apollo and Luna returned sample landing sites (Haskin and Warren, 1991; McKay et al., 1991); and (iv) compositions for lunar meteorite breccias (data from Wieczorek et al., 2006; Joy et al., 2010; Korotev, 2012). The soils from the feldspathic sites, i.e., Apollo 16 (A16) and Luna 20 (L20) are labelled.